JOURNAL OF MATERIALS SCIENCE 12 (1977) 1807–1826

Structural transformations produced during tempering of Fe-Ni-Co-Mo alloys

C. SERVANT, P. LACOMBE
Laboratoire de Métallurgie Physique, Université Paris-Sud, Centre d'Orsay, France

In an attempt to resolve the difficulties in interpreting the behaviour of the industrial maraging steel of VASCOMAX 300 type, we have studied the influence of separate or simultaneous additions of Co and Mo on the structural transformations taking place during the heating cycles at moderate rates (300° C h^{-1}) for the Fe–Ni base alloys. An interpretation of the mechanisms of the M → γ transformation, implying preponderantly diffusional mechanisms, has been proposed for the alloys Fe–Ni, Fe–Ni–Co, Fe–Ni–Mo and Fe–Ni–Co–Mo for which the Ni/Fe, Mo/Fe ratios are equal to those of the reference maraging steel. The ageing phenomena in the martensite of the alloys containing Mo have been studied and show the formation of G.P. zones having a diameter of a few tens of Å and spaced at an average distance of 120 Å, in the case of the quaternary alloy, at temperatures of 400 to 450° C.

1. Introduction

The structural transformations and mechanical properties of the Co–Mo maraging steels developed by Decker in 1962 [1] have been the object of several studies [2–9] during last few years. A complete interpretation of the observed phenomena, particularly those associated with the structural transformations, has been very difficult because of the very complex composition of these steels, such as VASCOMAX 300 (Composition in wt.%: 18.54 Ni; 8.94 Co; 4.85 Mo; 0.59 Ti; 0.12 Al; 0.050 Cu; balance: Fe), which is used as a reference in the text that follows.

We have therefore made a systematic study of the Fe–Ni alloys with successive and simultaneous addition of Co and Mo in an attempt to resolve these difficulties. These maraging steels have evoked a great deal of interest in the aerospace and aeronautical industries where they are used for missile framework and in landing chassis and in various other industries such as those manufacturing extrusion trains for light alloys, injection moulds for plastics, storage tanks for liquid gas, mechanical parts subjected to low temperatures, etc. [9]. The industrial applications of the maraging steels came from the mechanical properties, that can be developed by the ageing of the room temperature lath martensite structure obtained after suitably quenching these steels from the high-temperature austenitic condition.

In fact, after the usual ageing treatment at 480° C for 3 h [9] the rupture strength of the steel is of the order of 200 hbars, yet with a considerable ductility (≃ 10%).

The ageing is caused by the precipitation of Mo, Ti and Al in the form of intermetallic compounds [10]. In order to prevent the formation of the embrittling carbides, especially with titanium, the carbon content of these steels is kept low (0.02%). It is this low carbon content which renders the crystalline structure of the as-quenched martensite cubic, and not tetragonal as in the case of the hardened carbon steels, and therefore not metastable as in the latter case.

Firstly, we shall give a brief account of the methods of preparation of the synthetic steels of increasing complexity, tending towards that of the industrial steel which we have studied. We shall describe the various methods of investigation, which were conjointly used in an attempt to interpret as far as possible the behaviour of these alloys during reheating.

In the second part, we shall consider the role of Co and Mo in the structural transformations of the Fe–Ni alloys and also that of the simultaneous additions of the two elements.

In the third part, we shall deal with an analysis of the mechanism of the martensite–austenite transformation in alloys having following compositions (wt %):

78.34 Fe–21.66 Ni

66.6 Fe–18.4 Ni–15.0 Co

74.15 Fe–20.49 Ni–5.36 Mo

67.49 Fe–18.65 Ni–8.99 Co–4.87 Mo (Synthetic maraging steel)

18.54 Ni–8.94 Co–4.85 Mo–0.59 Ti–balance Fe (Industrial maraging steel), the Ni/Fe ratio of the synthetic alloys being equal to that of the industrial maraging steel.

Finally we shall discuss the pre-precipitation phenomena and precipitation produced in the martensite of the two synthetic alloys Fe–Ni–Mo and Fe–Ni–Co–Mo. As will be seen later, these phenomena condition the complex evolution of the subsequent $M \rightarrow \gamma$ transformation.

1.1. Preparation of the alloys and experimental methods

The alloys were prepared by solid-state sintering of high purity powders (characteristics are given in Table I) at very high temperatures ~ 1400° C, in an atmosphere of pure hydrogen [11]. Compared to the classical technique of melting and casting, this method offers an advantage since the alloys can be prepared easily at much lower temperatures, having a varying composition and yet preserving the respective proportions of their components. The principal impurity contents of the alloys thus operated were O_2 = 25 ppm, N_2 = 20 ppm, H_2 = 8 ppm, C = 36 ppm, S = 36 ppm. It may be noticed that the carbon content was much lower than that of the industrial maraging steel, which is of the order of 200 ppm.

The structural transformations of the different alloys have been studied simultaneously using dilatometry, differential thermal analysis, thermomagnetometry, thermoresistivity, X-ray diffraction at 20° C, small angle scattering of X-rays at 20° C, and optical and electron microscopy. In particular, dilatometry and thermomagnetometry offer the possibility of modifying the rate of heating within wide limits and so are well adapted for studying the influence of the rate of heating on the structural transformations. In the case of the alloys susceptible to ageing, the merit of the simultaneous use of dilatometry and thermoresistivity measurements was that the phenomena of precipitation and those of the formation of the austenite of reversion could be distinguished. Finally, small-angle scattering of X-rays and electron microscopy on thin foils provided us with additional information on the precipitation phenomena.

TABLE I

Powder	Origin		Chemical composition (wt %)	Average particle size (μm)
Iron	Office National des Industries de l'Azote	ex-carbonyl	Fe 99.8 – 99.9 C 0.05 O_2 0.10 N_2 0.01	4 – 5
Nickel	International Nickel Co	ex-carbonyl	C 0.05 – 0.10 O_2 0.10 Fe 0.01 S 0.001	4 – 7
Cobalt	Ugine Carbone	reduction of CoO_3 by H_2	Co 99.8 Ni 0.04 Fe 0.04 SiO_2 0.03 CaO 0.06	1.5 – 1.9
Molybdenum	Koch-Light Lab. Ltd		Mo 99.99 Fe 0.005 Ni 0.001 C 0.001 O_2 0.2	5.2

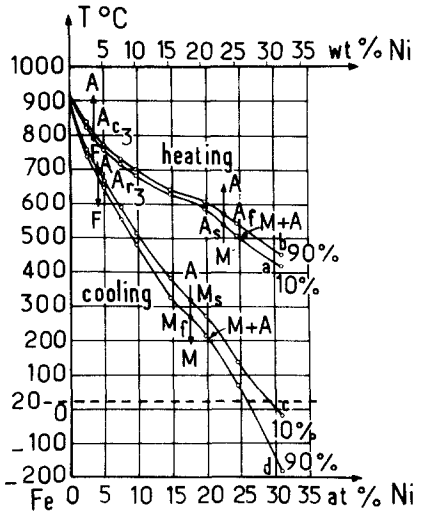

Figure 1 Experimental diagram by Jones and Pumphrey for the Fe–Ni binary system.

2. The role of Co and Mo in the structural transformations of the Fe–Ni alloys

2.1. The Fe–Ni system

The binary diagram Fe–Ni which served as a reference was not the equilibrium diagram, but its metastable form, established by Jones and Pumphrey in 1949 for a range of heating and cooling rates between 120 and 9000° C h^{-1} [12]. This diagram was redetermined in 1956 by Kaufman and Cohen for heating and cooling rates of 300° C h^{-1} [13]. Fig. 1 represents the phase diagram established by Jones and Pumphrey. Two important points may be noted from this diagram as functions of increasing nickel contents: (a) a simultaneous decrease in the transformation temperatures on heating (points A_{c_3} and A_s) and on cooling (points A_{r_3} and M_s)*. (b) an increase in the hysteresis between the transformation temperatures on heating and on cooling. In addition, the microstructure observed at 20° C after cooling from the high temperature γ region [14, 15] shows a marked evolution as a function of the increasing Ni contents.

The structure is equiaxed ferrite type for Ni contents ranging from 0 to 6 wt % and evolves towards an entirely lath-martensite structure ("Schiebung") [16] for Ni contents between 10 and 26 wt %. Beyond 26% Ni, the martensite transformation is not complete at 20° C and after quenching in liquid nitrogen and reheating at room temperature, one observes the formation of a lenticular martensite (twinned martensite, "Umklapp") [16], which consists of twin lenses having a characteristic habit plane and mid-rib [17, 18]. The lath martensite structure is shown in Fig. 2. The former γ grain boundaries and strongly disoriented blocks of laths are visible, with indented contours, terminating at these grain boundaries. This is obvious,

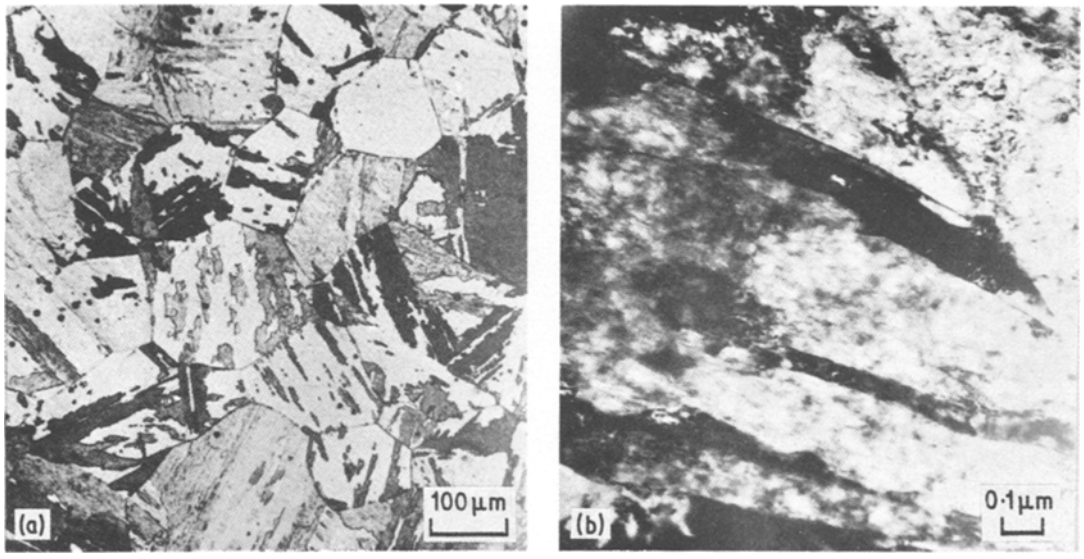

Figure 2 (a) Structure of the 78.34 Fe–21.66 Ni alloy after initial sintering at 1400° C for 2 h, observed on an optical microscope. (b) Structure of the same alloy observed on an electron microscope.

* A_{c_3} and A_s are the transformation points referring to equiaxed ferritic and martensitic structures during heating respectively and A_{r_3} and M_s are the transformation point referring respectively to ferritic and martensitic structures during cooling, respectively.

since there is an orientation relationship between the martensite and the austenite [19]. The laths may also show twinning relationships [20].

Electron microscopy reveals that each martensite lath is formed of bands either strongly disoriented (the bands showing twinning relationship) or weakly disoriented. Equally noticeable is a high dislocation density of the order of 10^{11} cm^{-2} [21].

For the Fe–Ni alloys having Ni content between 0 and 26%, the transformations $M \rightarrow \gamma$ and $\gamma \rightarrow M$ occur in a single step during heating and subsequent cooling in the range of 120 to 9000° C h^{-1}. This is shown by the differential dilatation curve with reference to alumina (Fig. 3a) for the binary alloy 78.34 Fe–2.66 Ni. The wt% ratio Ni/Fe for this alloy is 0.276, i.e. equal to the ratio of these elements in the reference "maraging steel" and therefore we chose the behaviour of this alloy as an illustration.

The transformation $M \rightarrow \gamma$ takes place with a drastic contraction of the order of 0.9%, whereas that of $\gamma \rightarrow M$ takes place with a dilatation of about 2%. That the transformations $M \rightarrow \gamma$ and $\gamma \rightarrow M$ take place in one single step are confirmed by means of differential thermal analysis (Fig. 3b).

2.2. The role of cobalt

The composition of the alloys investigated can be represented on the classical equilateral triangle (Fig. 4) by the method of Roozeboom [22]. The composition is obtained by drawing parallels to the sides of the triangle. We have chosen certain characteristic values of the Ni/Fe ratio:

0.064 to 0.111, corresponding, in the case of the metastable diagram of Jones and Pumphrey, to

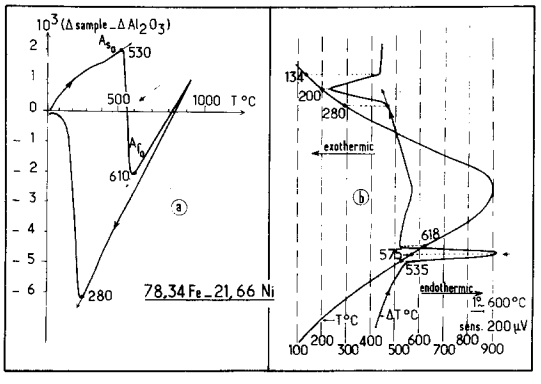

Figure 3 Structural evolution of the 78.34 Fe–21.66 Ni at heating and cooling rates of 300° C h^{-1} followed by (a) dilatometry (b) differential thermal analysis.

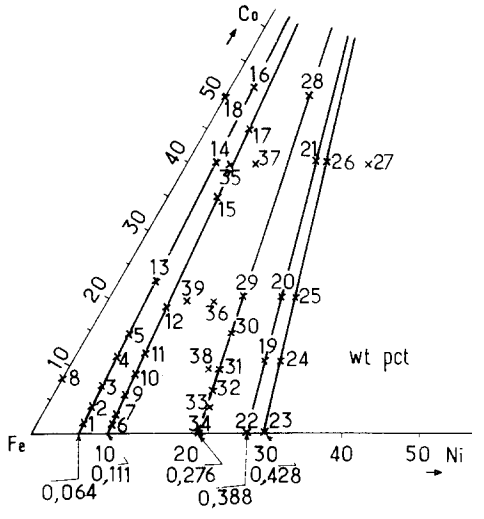

Figure 4 Composition of the Fe–Ni–Co ternary alloys (Roozeboom's representation).

the change-over from ferritic to the lath martensite structure;

0.276, corresponding to the Ni/Fe ratio of the reference maraging steel;

0.388 to 0.428, corresponding in the case of the binary diagram to the change-over from the lath martensite to the lenticular martensite structure.

In addition, the Co content was limited to 50 wt%. For all the Fe–Ni–Co alloys whose Ni/Fe ratio was constant and whose Co content increased, we noticed a shift towards higher transformation temperatures on heating and subsequent cooling as compared to that of the Fe–Ni alloys having the same Ni/Fe ratio (Fig. 5). On the other hand we observed a decrease in the hysteresis $\Delta T(A_{c_3} - A_{r_3})$ and $\Delta T(A_s - M_s)$ with increasing the Co content (Fig. 6).

We showed that the transformation $M \rightarrow \gamma$ takes place either in a single step or several steps, depending on the composition of the ternary Fe–Ni–Co alloy and the rate of heating. Fig. 7 represents the dilation curves, obtained in the course of heating and subsequent cooling at a rate of 300° C h^{-1} for Fe–Ni–Co alloys having a Ni/Fe ratio equal to 0.276. We noticed that when the cobalt content is low, the transformation $M \rightarrow \gamma$ was brought about in a single step as in the case of the binary Fe–Ni alloys, while with a Co content of about 9.45 wt%, the transformation $M \rightarrow \gamma$ was split (Fig. 7a, curve 31). The transformation $M \rightarrow \gamma$ took place over a wide range of temperatures and

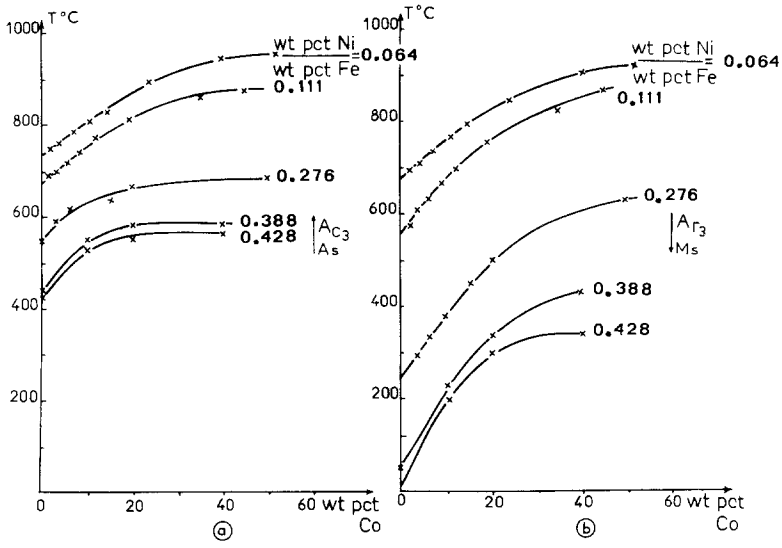

Figure 5 Variation of the A_{c_3}, A_s temperatures and A_{r_3}, M_s temperatures as a function of the increasing Co content for different Ni/Fe ratios.

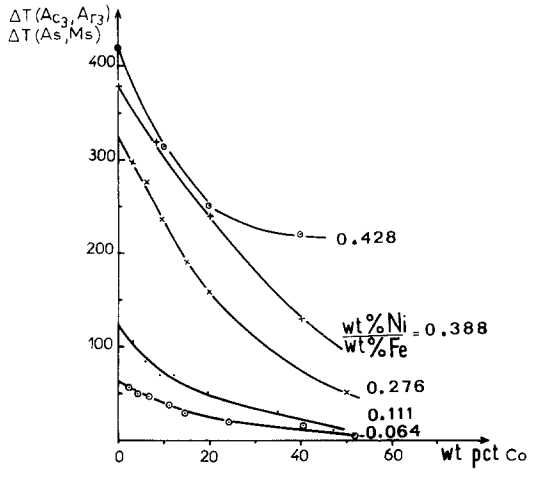

Figure 6 Variation of the hysteresis between the points A_{c_3}, A_{r_3} and between the points A_s, M_s as a function of the increasing Co content for different Ni/Fe ratios.

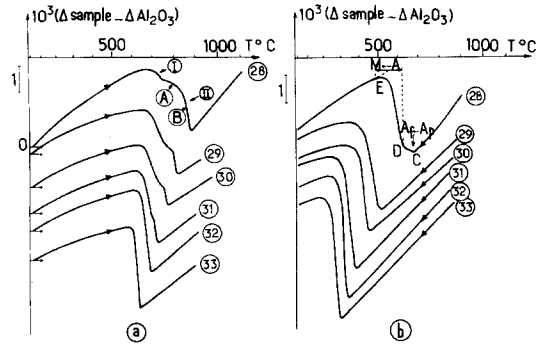

Figure 7 Dilation curves (at heating and cooling rates of 300° Ch^{-1} under an atmosphere of hydrogen) for Fe–Ni alloys with a Ni/Fe ratio = 0.276 (a) heating, (b) cooling.

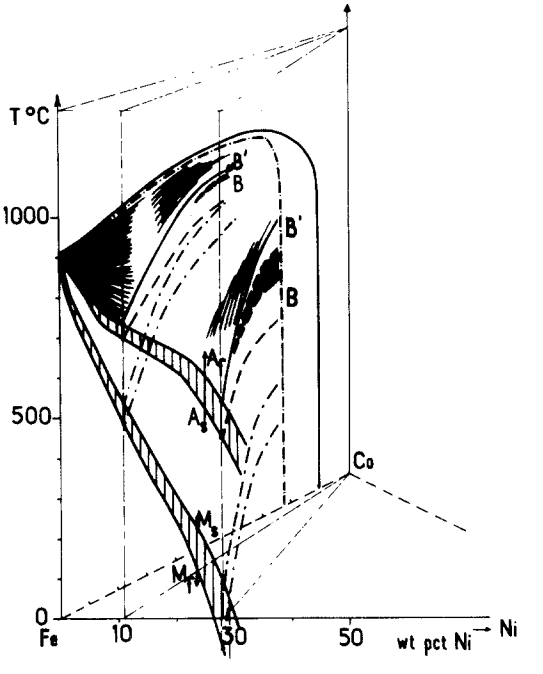

Figure 8 Ternary Fe–Ni–Co diagram.

the amplitude of the first step diminished as a function of increasing Co content.

On cooling (Fig. 7b), we observed either the martensite transformation alone, or an anomaly on the dilation curve associated with the Curie point of the austenite and then the transformation of this ferromagnetic austenite into martensite. With the help of the dilatometric results, we determined the ternary metastable Fe–Ni–Co phase diagram (Fig. 8). The binary diagrams forming the basis for the ternary Fe–Ni–Co phase diagram were the

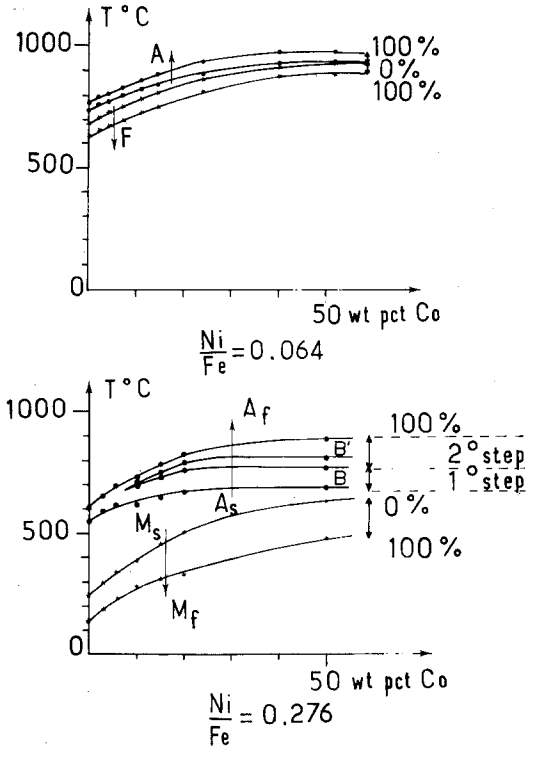

Figure 9 Vertical sections of the ternary Fe–Ni–Co diagram for different Ni/Fe ratios as a function of increasing Co content.

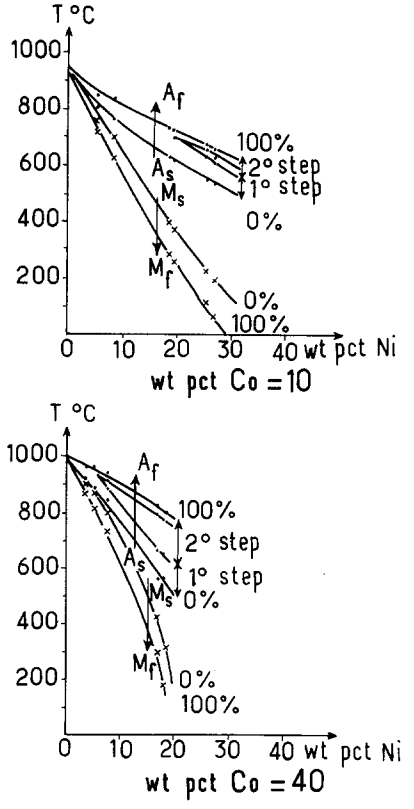

Figure 10 Vertical sections of the ternary Fe–Ni–Co diagram for different values of the cobalt contents as a function of increasing Ni wt %.

metastable diagram of Jones and Pumphrey for the binary Fe–Ni system, and the diagram published by Hansen [24] which is independent of the differences in the rates of heating and cooling in the range of 120 to 9000° C h^{-1} for the binary Fe–Co system. Vertical sections for different Co contents and with different values for the Ni/Fe ratio are represented in the Figs. 9 and 10.

Regarding the second stage of the transformation $M \rightarrow \gamma$ we have represented on these vertical sections, two domains A and B corresponding to a progressive contraction representing the passage from the first to the second step A, which in its turn is marked by a sudden contraction B (Fig. 7). It will be noticed that the transformation $M \rightarrow \gamma$ is not split unless the sum of the elements (Ni + Co) is sufficient. Thus, for 40 wt % of Co, 6 to 7 wt % of Ni is sufficient to split up the transformation.

2.3. The role of molybdenum

We studied a more restricted range of composition for this element than in the case of the ternary Fe–Ni–Co system (Fig. 11), in order to avoid the formation of intermediate phases with increasing molybdenum contents.

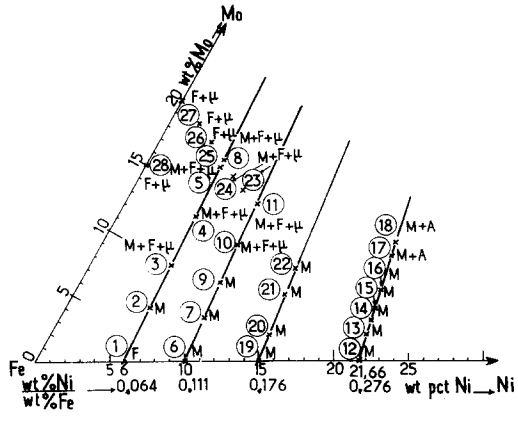

Figure 11 Composition and structure at 20° C of the Fe Ni Mo alloys prepared by sintering (Roozeboom's representation).

X-ray diffraction analysis showed several single-phase or multiple-phase regions at 20° C, designated by the notations:

F

$F + \mu$

$F + \mu + M$

$F + M$

M

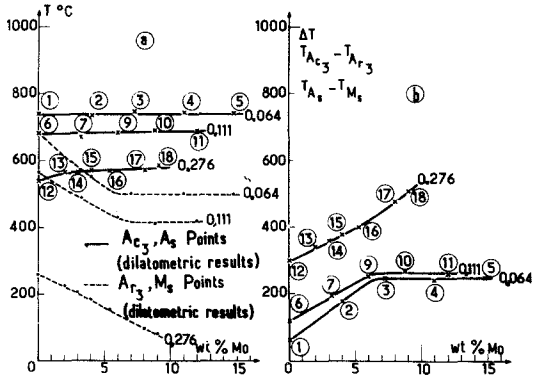

Figure 12 (a) Variation of the A_{c_3}, A_s temperatures and A_{r_3}, M_s temperatures as a function of increasing Mo contents for different Ni/Fe ratios. (b) Variation of the hysteresis between the points A_{c_3}, A_{r_3} and between the points A_s and M_s as a function of the increasing Mo contents for different values of Ni/Fe ratio.

where F = ferrite, M = martensite, $\mu = Fe_7Mo_6$.

For a constant Ni/Fe ratio and an increasing percentage of Mo, we noticed (Fig. 12a) a very slight elevation of the transformation temperature on heating, A_{c_3} or A_s, and a considerable fall in the transformation temperature on cooling, A_{r_3} or M_s, contrary to what is observed when Co is added to the Fe–Ni system.

The hysteresis ΔT between the transformation temperatures $A_{c_3} - A_{r_3}$, $A_s - M_s$, increased (Fig. 12b) the opposite of what happened when Co was added the binary Fe–Ni system. The fact that the transformation temperatures obtained for the alloys where the values for the Ni/Fe ratio = 0.064 and 0.111 and whose Mo content is of the order of 6 to 7 wt % are constant, confirmed that these alloys represent a three phased region F + M + μ. In fact, only the proportion of the three phase changes for the alloys of different composition in the three phase region, their composition remaining unaltered (the temperatures of transformation are therefore identical).

It was shown that the transformation M → γ takes place in a single or several successive steps according to the composition of the ternary Fe–Ni–Mo alloy and the rate of heating. Fig. 13a represents the dilation curves for the Fe–Ni–Mo alloys whose Ni/Fe ratio is equal to 0.276 for increasing Mo contents. These curves were recorded for heating and cooling rates of 300° C h^{-1}. The transformation M → γ is split, starting from a Mo content of a 4 wt %. The second step is characterized by a much smaller contraction than that observed for the ternary Fe–Ni–Co alloys.

On the differential thermal analysis curves (Fig. 13b) the first step is characterized by a well defined endothermic peak. The second step is progressively better defined as the percentage of Mo increases. By the same method, we observe before

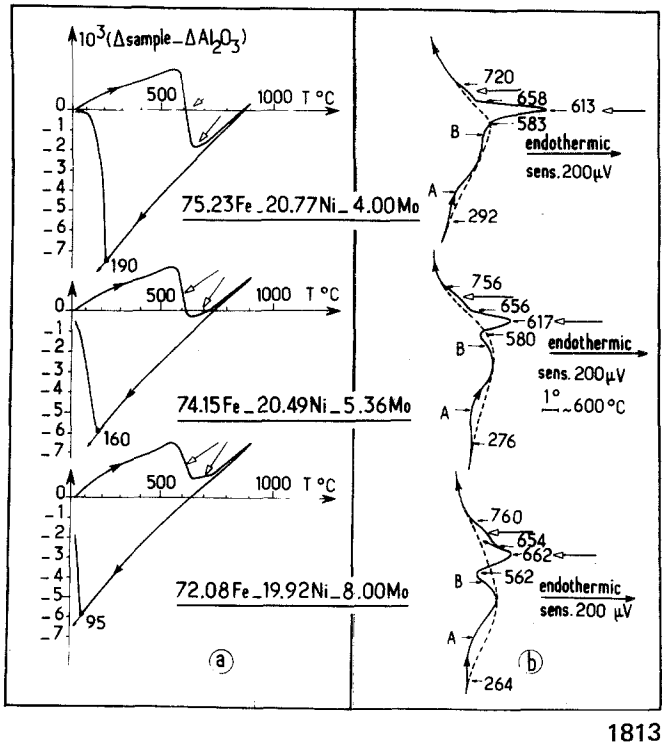

Figure 13 Structural evolution of the Fe–Ni–Mo alloys number 15, 16 and 17 at a heating and cooling rate of 300° C h^{-1} : (a) by dilatometry, (b) by differential thermal analysis.

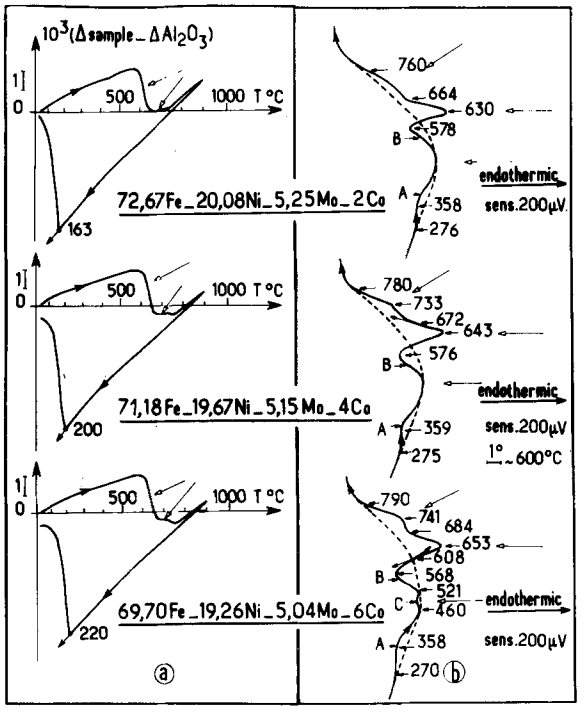

Figure 14 Structural evolution of Fe–Ni–Co–Mo quaternary alloys at heating and cooling rates of 300° C h^{-1}. (a) by dilatometry, (b) differential thermal analysis.

the point A_s two exothermic peaks marked A and B, whose resolution increases with the increasing Mo contents. We previously interpreted these peaks as being a single endothermic peak as was also proposed by Nam Bui *et al.* [42] and Maeder [26] for the reference maraging steel; this was due to several possibilities of tracing the reference line on the thermal analysis curves.

The microcalorimetric curves plotted at a rate of 90° C h^{-1} under the atmosphere of hydrogen have in fact enabled us to confirm that the processes occurring before the A_s point are exothermic and this eventually enabled us to trace the reference lines for the differential thermal analysis recording.

In the range of temperature corresponding to these peaks, one observes an increase in the hardness but a slight fall in the resistivity. These two peaks were associated with the precipitation involving Mo in martensite, as was later confirmed by small-angle X-ray scattering studies [39].

2.4. The effect of the simultaneous addition of Co and Mo

Cobalt was added in an increasing quantity to the alloy of composition 74.15 Fe–20.49 Ni–5.36 Mo whose Ni/Fe and Mo/Fe ratios are equal to that of the reference maraging steel. Fig. 14a shows that the transformation $M \rightarrow \gamma$ at a heating rate of 300° C h^{-1} takes place in two successive steps. The second step was characterized by a more and more pronounced contraction as the Co content increased. At the same time, differential thermal analysis (Fig. 14b) showed the appearance of a third exothermic peak of low amplitude (marked C) with increasing cobalt contents. For a Co content of 8.99 wt%, the quaternary synthetic maraging steel was obtained. The transformation $M \rightarrow \gamma$ was observed to take place during the dilatometric analysis with two very prominent contractions (Fig. 15a) and was characterized by two

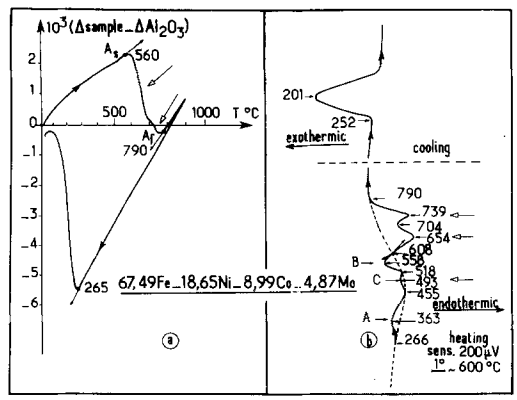

Figure 15 Structural evolution of the synthetic maraging steel prepared by the sintering process at heating and cooling rates of 300° C h^{-1}: (a) by dilatometry, (b) by differential thermal analysis.

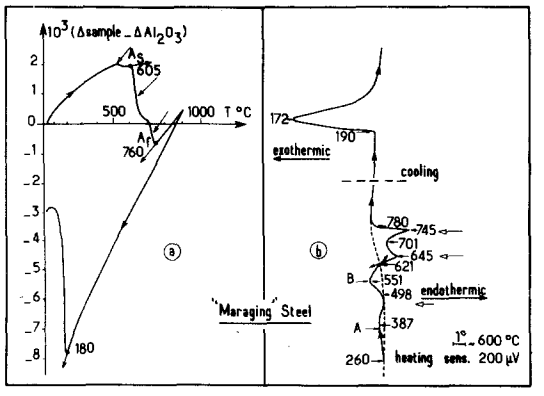

Figure 16 Structural evolution of the industrial maraging steel at heating and cooling rates of 300° C h^{-1} (a) by dilatometry, (b) by differential thermal analysis.

well defined endothermic peaks on differential thermal analysis (Fig. 15b). The precipitation step is achieved in three well-defined exothermic peaks A, B and C.

A comparison of the structural evolution of the industrial maraging steel (Fig. 16a) and that of the quaternary synthetic alloy, reveals essentially a difference in their behaviour before reaching the point A_s. In fact, the dilation curve of the industrial steel presents a distinct contraction of low amplitude before attaining the point A_s compared to the synthetic alloy. This was attributed to the formation of incoherent precipitates of the type Ni_3Mo, Ni_3Ti [25, 26]. On the other hand, on differential thermal analysis curves, the peak C observed for the synthetic alloy is not visible. However, in the case of the industrial steel, which contains precipitating elements other than Mo, i.e. Ti and Al, it is believed that the different processes of precipitation or pre-precipitation interfere and that the peaks A and C are not resolved (Fig. 16b).

In conclusion, for the systems Fe–Ni, Fe–Ni–Co, Fe–Ni–Mo and Fe–Ni–Co–Mo, the study of the variations of the points A_s and M_s led us to trace a part of the diagrams of these systems, valid at least for heating and cooling rates of 300° C h^{-1}. In addition this study allowed us to interpret the mechanisms of the transformation $M \rightarrow \gamma$, as will be seen in the following section.

3. The mechanisms of the transformation $M \rightarrow \gamma$

For the four alloys having the following composition (wt %)
78.34 Fe–21.66 Ni
66.6 Fe–18.4 Ni–15.0 Co
74.15 Fe–20.49 Ni–5.36 Mo
67.49 Fe–18.65 Ni–8.99 Co–4.87 Mo we made an attempt to determine the precise mechanisms involved in each of the stages of the transformation $M \rightarrow \gamma$. With the exception of ternary Fe–Ni–Co alloy, these alloys had ratios of Ni/Fe, Mo/Fe and Co/Fe equal to that of the reference maraging steel. The alloy with the composition 70.95 Fe, 19.06 Ni and 9.45 Co which satisfies this last condition constitutes the limit of the evolution of the transformation $M \rightarrow \gamma$ in two distinct steps (Fig. 7a, curve 31); we preferred to choose the 66.6 Fe–18.4 Ni–15.0 Co alloy for which the evolution on heating takes place in two well defined steps (Fig. 7a, curve 32).

For this, different specimens were heated (at a rate of 300° C h^{-1}) to different temperatures within

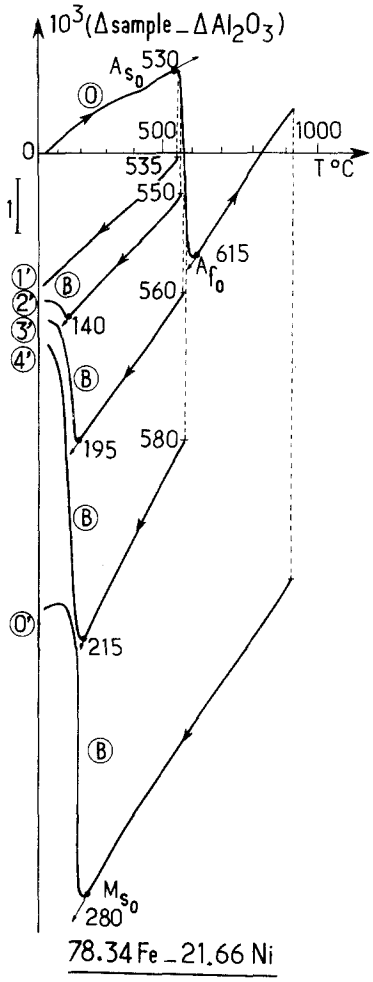

Figure 17 Dilation curves of the Fe–Ni alloy during cooling (at 450° C h^{-1}) from different temperatures in the austenitic transformation range.

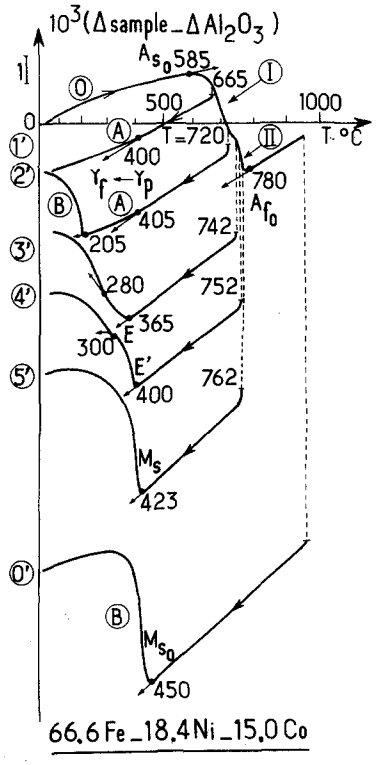

Figure 18 Dilation curves of Fe–Ni–Co alloy during cooling (at 450° C h^{-1}) from different temperatures in the austenitic transformation range.

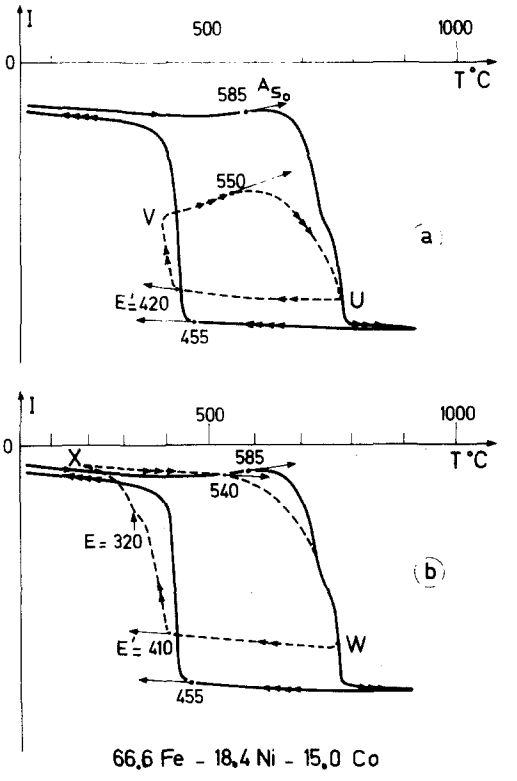

Figure 19 Thermomagnetic curves for the Fe–Ni–Co alloy showing that the transformation beginning at points E′ and E are martensitic.

the limits in which the transformation to austenite is brought about. They were then cooled down to room temperature at an average rate of 450° C h^{-1}, and afterwards reheated up to 900 to 1000° C (at a rate of 300° C h^{-1}) in order to study the effect of an incomplete martensitic transformation on subsequent austenite formation [23]. Hereafter, we shall give the index 0 to the curves and the points of transformation of the specimens undergoing a primary thermal cycle subsequent to homogenization of the γ phase. The temperature at which the reversion of the martensite into austenite, between the points A_{s_0} and A_{f_0}, is stopped will be referred to as "T_R".

3.1. Experimental results

3.1.1. 78.34 Fe–21.66 Ni alloy

It can be seen from Fig. 17, that if T_R is slightly above A_{s_0}, no transformation is observed during cooling (curve 1′), if T_R increases to a value between A_{s_0} and A_{f_0}, a single martensitic transformation takes place for which the M_s temperature is lower than M_{s_0} and increases tending towards M_{s_0} (curves 2′ to 4′).

3.1.2. 66.6. Fe–18.4 Ni–15.0 Co alloy

The tranformation $M \rightarrow \gamma$ was brought about in two successive steps (Fig. 18). When T_R is situated in the first stage (I), we had either simply the Curie transformation of the austenite formed between the point A_{s_0} and T_R (curve 1′) (with the help of thermomagnetic analysis we were able to show that this para-ferromagnetic transformation extends over a wide range of temperatures, reaching 300° C, leaving one to suppose that a considerable variation occurs in the nickel content of the austenite) or the Curie transformation of the austenite followed by the transformation into martensite of this ferromagnetic austenite, at a temperature below the point M_{s_0} (curve 2′). When T_R fell in the second step (II) of the transformation $M \rightarrow \gamma$, a split transformation was observed for which the E and E′ points are below M_{s_0} (curves 3′ and 4′). Thermomagnetic analysis has shown that these two transformations beginning respectively at the points E and E′ are irreversible and correspond to the formation of two martensitic phases differing in their Ni and Co content (Fig. 19). The first part of the figure, in fact, relates to a

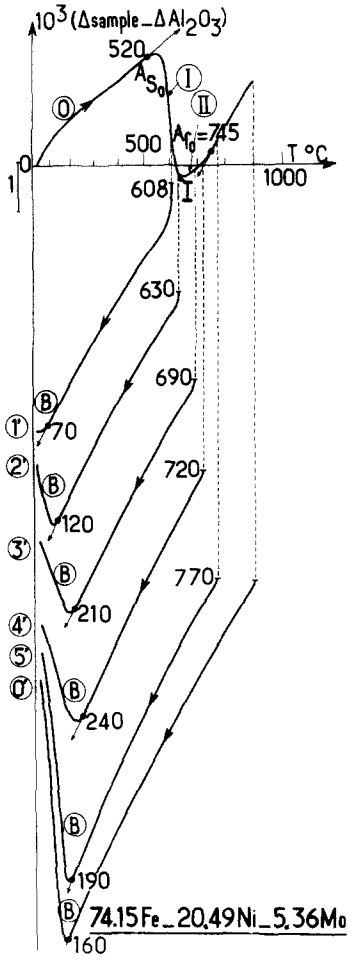

Figure 20 Dilation curves for the Fe–Ni–Mo alloy during cooling (at 450° C h^{-1}) from different temperatures in the austenitic transformation range.

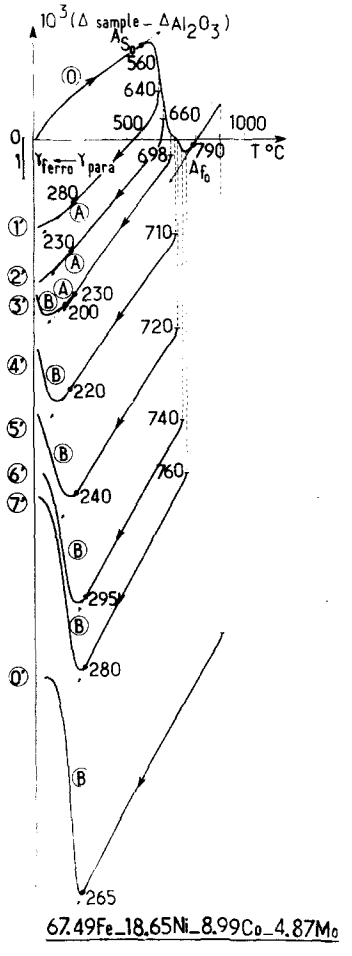

Figure 21 Dilation curves for the synthetic maraging steel during cooling (450° C h^{-1}) from different temperatures in the austenitic transformation range.

specimen of Fe–Ni–Co heated at a rate of 300° C h^{-1} to the point U, then cooled at a rate of 600° C h^{-1} up to the point V. During this cooling appears a transformation beginning at the point E′. The curve obtained on reheating at 300° C h^{-1} does not coincide with the curve UV. Beyond 550° C, an irreversible transformation corresponding to the transformation of martensite into austenite (point E′ on Fig. 19) is observed. Fig. 19b figure corresponds to a similar treatment given after the second transformation beginning at the point E.

3.1.3. Alloys having Ni/Fe and Ni/Mo ratios equal to that of the maraging steel: 74.15 Fe–20.49 Ni–5.36 Mo and 67.49 Fe–18.65 Ni–8.99 Co–4.87 Mo

The transformation M → γ for these two alloys takes place in two distinct steps (Fig. 20 and 21. When T_R lies in the first step we observed on cooling, either only the Curie transformation of the austenite formed between the points A_{s_0} and T_R, Fig. 21, curve 1′ (this transition extends over a wide range of temperatures as in the case of the austenite formed between the points A_{s_0} and T_R for the Fe–Ni–Co alloy, Fig. 17, curve 1′), or the Curie transformation of the austenite, followed by the martensitic transformation of this austenite having its M_s point always lower than M_{s_0} (Fig. 21, curve 3′); when T_R is situated in the second step, we observed a single martensitic transformation spread over a range of temperature for which the M_s point is distinctly above the M_{s_0} point. For example, for the Fe–Ni–Mo alloy, the Fig. 20 shows that the difference between the points M'_{s_4} and M'_{s_0} is equal to +80° C. The fact that the M_s

point lies above M_{s_0} in the second step of the $M \rightarrow \gamma$ transformation was attributed to the presence of molybdenum.

3.1.4. Industrial maraging steel

For this steel, one observes the same phenomena as those for the quaternary alloy Fe–Ni–Co–Mo with one exception, i.e. the observed M_s points are always below or equal to the point M_{s_0} (Fig. 22) for a cooling rate of $450^\circ C\,h^{-1}$.

3.1.5. Effect of the rate of cooling from T_R

In order to verify that the observed variations of the point M_s was solely due to the evolution of the alloys produced during the heating process between 20° C and T_R, we varied the cooling rates widely. Fig. 23 shows that for the Fe–Ni alloy, the dilation curves 1′ and 1″ obtained on cooling at $5^\circ C\,min^{-1}$ and $600^\circ C\,min^{-1}$ give identical M_s points below M_{s_0}. Therefore, it can be concluded that the Fe–Ni alloy does not undergo any structural evolution during cooling from the temperature T_R and that the variation observed in the M_s points are due to the transformation produced on heating between the points A_{s_0} and T_R. The same results were obtained for the Fe–Ni–Co alloy. For the alloys containing Mo, there is a slight tendency for homogenization of the constituents of the phases formed during the $M \rightarrow \gamma$ transformation produced during cooling (from the temperature T_R) which we shall discuss later.

It is this phenomenon of rehomogenization during cooling at moderate rates ($\simeq 450^\circ C\,h^{-1}$) that explains the observation of the M_s points below or equal to M_{s_0} in the case of the maraging steel. For this steel, Maeder [26] determined the values of M_s which are 75° C above that of M_{s_0}, on cooling at $1800^\circ C\,min^{-1}$.

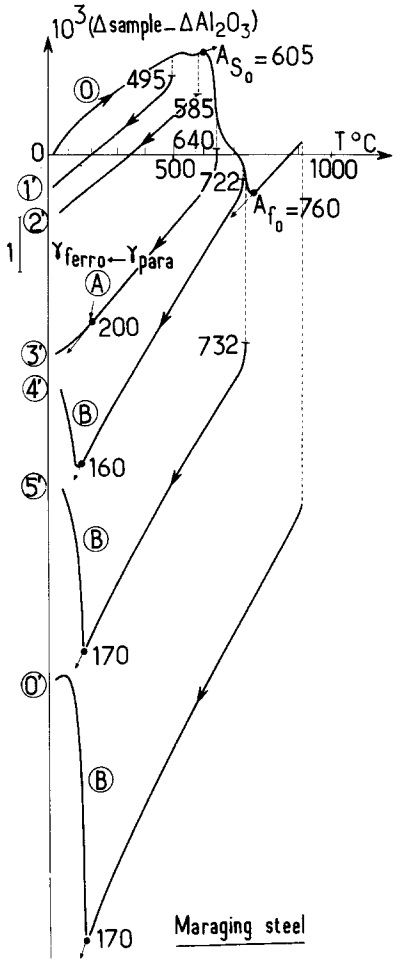

Figure 22 Dilation curves for the industrial maraging steel during cooling (at $450^\circ C\,h^{-1}$) from different temperatures in the austenitic transformation range.

3.2. Interpretation of results

3.2.1. Fe–Ni alloy

For this alloy we were able to determine in the course of the reheating cycle after cooling from T_R the variations in the points M_s and A_s. These points are always below M_{s_0} and A_{s_0}. No Curie point was observed in the range 1000 to 20° C showing that the austenite formed by the transformation $M \rightarrow \gamma$ has a nickel content < 30 wt%. In fact, according to Hansen [27], for nickel contents between 30 and 100 wt%, the austenite shows a Curie point above 20° C. The following interpretation is proposed for the transformation $M \rightarrow \gamma$. Martensite with an equal Ni and C_0 content decomposes by a diffusional mechanism in two phases having different crystallographic structures and nickel contents, according to following process which represents the return towards the equilibrium state.

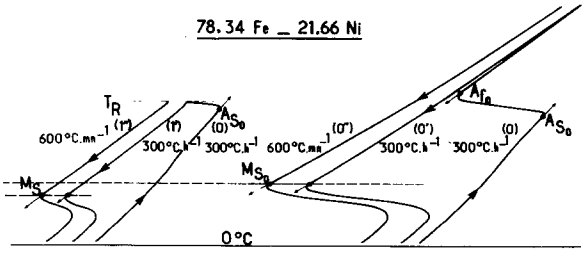

Figure 23 Influence of the cooling rate on the temperature of the M_s point.

$$\begin{array}{ccccc} M \rightarrow & M_p & + & \gamma_R & \\ C_0 & C_{M_p} < C_0 & & c_{\gamma_r} > c_0 & \end{array} \quad (1)$$

where M_p is a martensitic phase depleted in Ni content and γ_R is a austenitic phase enriched in Ni content. Between the points A_{s_0} and A_{f_0} the evolution of the points representing the two phases M_P and γ_R are represented schematically in Fig. 24a.

This difference in the Ni content of the two phases M_P and γ_R could not be confirmed by Castaing's microprobe analysis because of the very small size of closely knitted plates of γ_R and M_P, which is much below the resolving power of the microprobe. However the interpretation based on the diffusion mechanism during the austenite transformation has been confirmed by treatments similar to those employed by Maeder [26], i.e. heating up to T_R and then cooling to 20° C, at a rate of 800° C min^{-1}, for the same alloy. In fact, the author does not observe any significant variation in M_s during cooling from different T_R temperatures. During rapid heating, the diffusion phenomena in the $M \rightarrow \gamma$ transformation were minimized, then nullified, beyond a critical heating rate (1350° C min^{-1}), thus accounting for the constant M_s values.

Confirmation was also supplied by the work of Krauss and Cohen [28] on the Fe–33 Ni alloy. These authors have carried out treatments similar to ours i.e. slow (300° C h^{-1}) and rapid heating. Only in the case of slow heating have they found a significant increase in the parameter of the austenite corresponding to an enrichment in nickel.

Priester [29] further confirmed our results by the potentiokinetic method and concluded that it was due to a preferential accumulation of Ni at the interface between the martensite and the austenite plates.

3.2. Fe–Ni–Co alloy

For this alloy, we observed M_s and A_s points were always below M_{s_0} and A_{s_0} points and that a Curie transformation of the austenite which extends over a wide range temperatures (300° C) thus reflecting the heterogeneity in the composition of the austenite.

Two M_s points were found below M_{s_0}, where T_R is situated in the second stage of the $M \rightarrow \gamma$ transformation and the metastable ternary Fe–Ni–Co diagram showing a decrease in the A_s and M_s points when the Ni content rises, the Co/Fe ratio remaining constant.

The first step of the transformation $M \rightarrow \gamma$ is interpreted in the same way as for the binary alloy.

$$M \rightarrow M_P + \gamma_R$$

During the second step the M_P phase formed in the first step is decomposed by the same process (Fig. 24b).

$$M_P \rightarrow M'_P + \gamma'_R$$

with

$$C_{M'_P} < C_{M_P} < C_0 \quad \text{and} \quad C_0 < C_{\gamma'_R} < C_{\gamma_R}$$

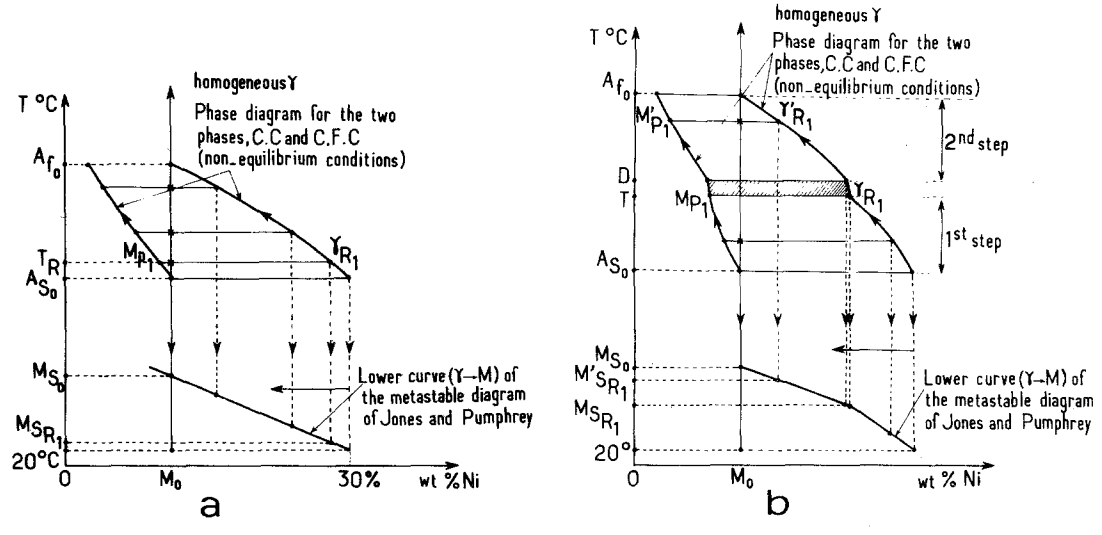

Figure 24 Schematic representation of the martensite during the treatment of the slow anisothermal reversion (300° C h^{-1}): (a) alloy 78.34 Fe–21.66 Ni, (b) alloy 66.6 Fe–18.4 Ni–15.0 Co.

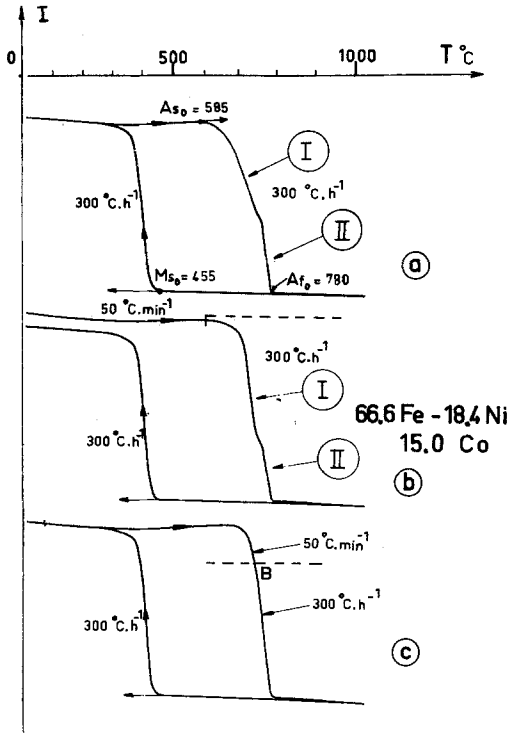

Figure 25 Thermomagnetic curves for the alloy Fe–Ni–Co showing that the slowing down of the austenitic transformation between two steps is related to the evolution taking place during the first step.

The experiments which follow confirm the fact that the second step is associated with the decomposition of the M_P phase formed in the first stage.

In Fig. 25, we have represented the variations in the intensity of magnetization I as a function of increasing temperature. The curve (a) represents the heating at 300° C h^{-1} from 20 to 1000° C. The transformation $M \rightarrow \gamma$ takes place in two clearly distinct steps. The curve (b) represents the heating at 50° C h^{-1} up to the point A_{s_0} followed by a heating at 300° C h^{-1} up to 1000° C. The two steps of the transformation are still clearly distinct. The curve (c) represents the heating at 50° C min^{-1} up to point B: this corresponds approximately to the diminution of the magnetization corresponding to half of the first step, followed by heating at 300° C h^{-1} up to 1000° C. A single step is observed. The same curve comprising a single step is obtained when the heating is carried out at 50 C min^{-1} continuously between 20 and 1000° C. This heating of the Fe–Ni–Co alloy at 50° C min^{-1} up to point B minimises the diffusion phenomena normally occuring in the first stage at 300° C h^{-1}. Thus the phase M_P is not much impoverished in Ni as compared to the initial martensite. It does not give rise to a transformation starting from a temperature distinctly higher than the point T on Fig. 18.

These fact suggest that a shear mechanism during the transformation $M \rightarrow \gamma$ does not become preponderant unless heating is carried out at very high rates.

3.3. The Fe–Ni–Mo and Fe–Ni–Co–Mo

In the case of these alloys, we showed by electron microscopy and small-angle X-ray scattering studies [39] that during heating at 300° C h^{-1}, a precipitation takes place in the martensite before reaching the point A_{s_0}. This precipitation brings about a heterogeneity in the composition of the martensite. Variations in the M_s points are observed during cooling from the temperature T_R, situated in the first and second step of the $M \rightarrow \gamma$ transformation, and from these variations one can separate the martensite into zones either rich in (Ni + Mo) or depleted in (Ni + Mo), denoted by M_R and M_P respectively.

The first step of the transformation $M \rightarrow \gamma$, for which M_s points have been found to be always below M_{s_0}, represents the transformation of the phase M_R according to the following process.

$$M_R \rightarrow M_{RP} + \gamma_{RR}$$

The second step of this transformation, having M_s values superior to M_{s_0} represents the transformation of both phases.

$$M_{RP} \rightarrow M_{RPP} + \gamma_{RPR}$$

and

$$M_P \rightarrow M_{PP} + \gamma_{PR}$$

with

$$C_{\gamma PR} < C_0 < C_{\gamma RPR} < C_{\gamma RR}$$

We confirmed this interpretation of the $M \rightarrow \gamma$ transformation, implying a diffusion mechanism by modification in the rate of heating, either throughout the heating process between 20 and 1000° C, or beyond certain temperatures between the points A_{s_0} and A_{f_0} by cumulative thermal cycles between 20° C and a temperature T_R [30], with the purpose of increasing the difference in the composition between the various phases formed during each cycle following the process (1). Finally for all the alloys studied, we showed that the $M \rightarrow \gamma$ transformation takes place at moderate rates of about 300° C h^{-1} by a mechanism which is mainly diffusional in nature. The difference in the composition of the different phases formed during the

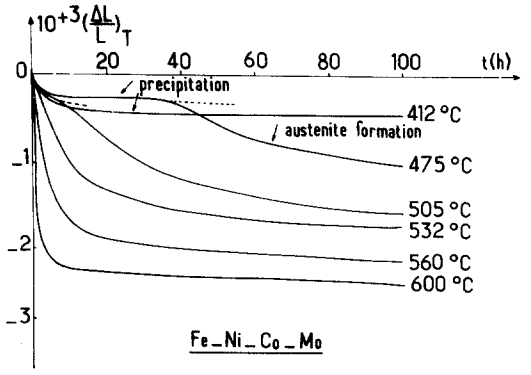

Figure 26 Isothermal dilation curves (under hydrogen atmosphere) for 67.49 Fe–18.65 Ni–8.996–4.87 Mo alloy.

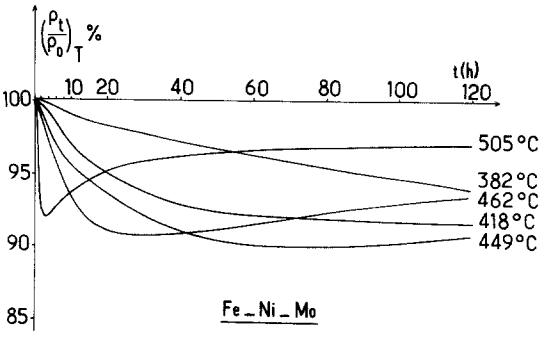

Figure 27 isothermal thermoresistivity curves (under hydrogen atmosphere) for 74.15 Fe–20.49 Ni–5.36 Mo alloy.

transformation is greatest at the beginning of the transformation.

The intervention of a competitive shear mechanism is not ruled out. However, none of the experimental methods we used was able to reveal this.

In the case of the Fe–Ni–Mo and Fe–Ni–Co–Mo alloys, the formation of the preprecipitates and precipitates before the point A_{s_0} condition the subsequent $M \rightarrow \gamma$ transformation; therefore we have studied the ageing phenomena produced in the martensite under isothermal conditions.

4. Ageing phenomena produced in the martensite of the Fe Ni Mo and the Fe Ni Co Mo alloys

The dilation curves for the quaternary alloy are represented in Fig. 26. They show that:

at temperatures of 400° C, a slight contraction is produced which represents the precipitation in the martensite. After 100 h of ageing, this contraction remains very small, of the order of 5×10^{-4};

between 450 and 500° C, the initial small contraction corresponding to the precipitation is followed by a much greater one due to the formation of reversed austenite under isothermal conditions;

at the ageing temperature above 500° C, the two former phenomena are no longer distinct. The thermoresistivity measurements allow a better separation of the two phenomena, precipitation and the formation of reversed austenite as is shown in Fig. 27, relative to the ternary alloy;

at temperature below 450° C, we observe a progressive decrease in the resistivity indicating the precipitation in one single step;

at temperature above 450° C, a more drastic and greater decrease in the resistivity, corresponds to the precipitation in a single step followed by an increase in this parameter which in turn represents the formation of the reversed austenite. Fig. 28 shows the curves obtained by this method for the quaternary alloy;

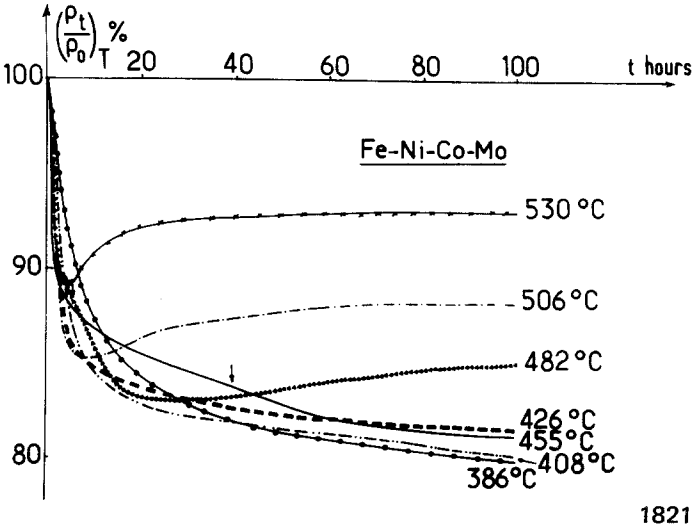

Figure 28 Isothermal thermoresistivity curves (under hydrogen atmosphere) for 67.49 Fe–18.65 Ni–8.99 Co–4.97 Mo alloy.

at the temperatures below 450° C, the precipitation takes place in a single step. The fraction precipitated is much greater than that in the case of the ternary alloy;

between 450 and 500° C, the precipitation takes place in two successive steps (see curve at 455° C);

at temperature above 500° C, the precipitation once again takes place in a single step and is followed by the formation of the reversed austenite.

The nature of the experimental curves as well as study of the theoretical models (Cottrell and Bilby [32], Harper [33]) led us to propose that the most probable equation is that of Johnson and Mehl [31]:

$$Y(t) = 1 \exp(-kt^n) \qquad (2)$$

In this equation $Y(t)$ represents the fraction transformed after time t and is expressed in the form

$$Y(t) = \frac{\rho_0 - \rho_t}{\rho_0 - \rho_\infty}$$

therefore Equation 2 becomes

$$\rho_t = \rho_\infty - (\rho_0 - \rho_\infty) \exp(-kt^n)$$

However, the value ρ_∞ is never attained experimentally owing to the duration of ageing being limited to about 100 hours, and the formation of the reversed austenite.

We have therefore used computer calculation in order to determine the three unknown values ρ_∞, k and n, so that the theoretical curve fits well with the experimental one as far as possible.

The results obtained for the ternary alloy are represented in Table II;

the values of parameters n and k increase almost regularly as a function of the increasing temperature;

at the lowest ageing temperature (380° C) n is equal to 0.75 which is quite close to that of $\frac{2}{3}$ obtained by theoretical models mentioned earlier, for which the precipitation is localized on the dislocations. This has been confirmed by the examination of thin foils by transmission electron microscopy (Fig. 29).

TABLE II

T(°C)	n	$k(t^{-n})$	$k(t^{-1})$
382	0.76	0.01	0.003
418	1.13	0.03	0.07
442	0.93	0.08	0.06
462	1.39	0.07	0.14
505	1.95	0.72	0.85

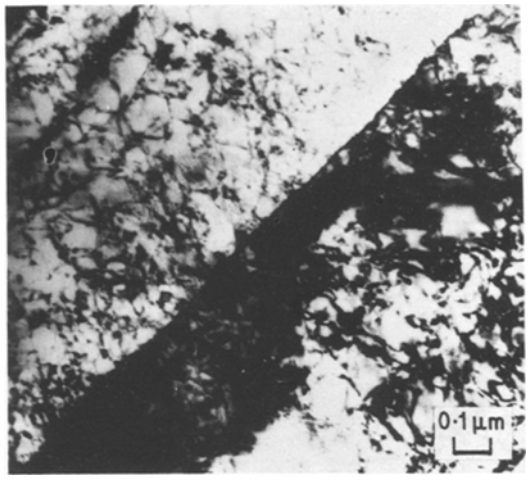

Figure 29 Structure of the alloy 74.15 Fe–20.45 Ni–5.36 Mo held at 382° C for 100 h, observed by electron microscopy.

For ageing temperatures above 450° C, we observe spherical precipitates and long patches of reversed austenite (Fig. 30). We have determined [34] the apparent activation energy of the precipitation Q, assuming the rate of the reaction equal to

$$\frac{dY}{dt} = A \exp -\frac{Q}{RT}$$

where A is a constant independant of the temperature. For a fraction transformed, $Y(t) =$ constant, it becomes

$$\mathrm{Log}\frac{t}{n} \propto \frac{Q}{RT}$$

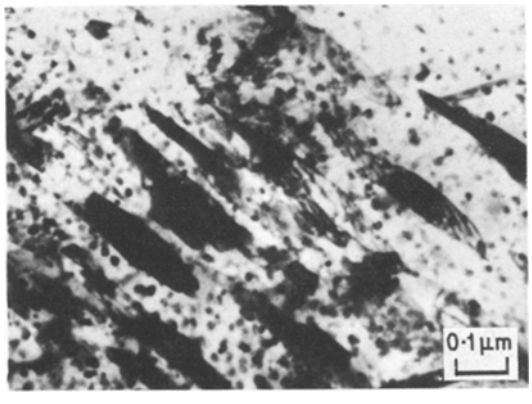

Figure 30 Structure of the 74.15 Fe–20.45 Ni–5.36 Mo alloy observed by electron microscopy showing the reversed austenite in the form of elongated patches.

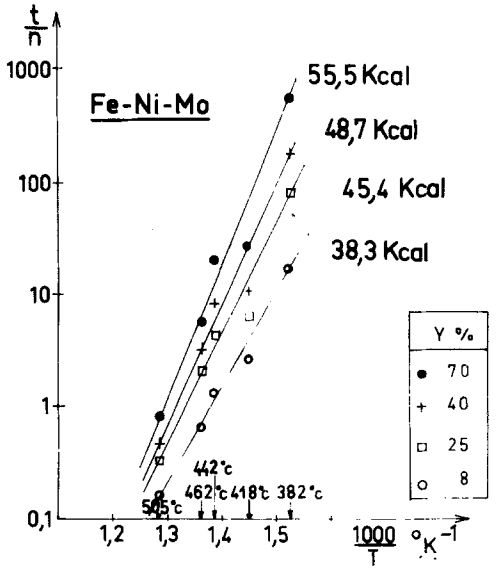

Figure 31 Apparent activation energy of precipitation for different values of the fraction transformed in the case of the 74.15 Fe–20.49 Ni–5.36 Mo alloy.

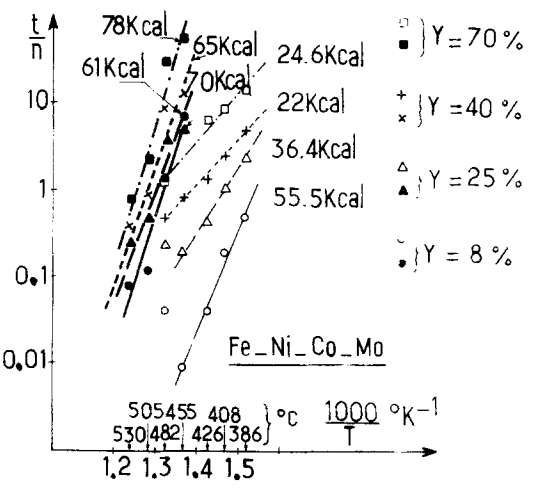

Figure 32 Apparent activation energy by precipitation for different values of the fraction transformed in the case of the 67.49 Fe–18.65 Ni–8.99 Co–4,87 Mo alloy.

Expressed as a function of $\frac{1}{T}$, this should give straight lines with slope $\frac{Q}{R}$, which is confirmed by Fig. 31. We observe that, when the fraction transformed is small, for example 8%, Q is about 38 kcal mol^{-1}. This value is much below the value obtained for the activation energy of the diffusion of molybdenum in α iron, which is about 57 kcal mol^{-1}. The large network of dislocations is a factor which helps diffusion. This is the phenomenon of "pipe diffusion".

In the case of quaternary alloys, the values of k and n of the Equation 2 are given in Table III and the evolution of Q as a function of the fraction transformed is illustrated in Fig. 32. We observe two sets of straight lines leading to two values of Q representing two stages of precipitation revealed by the thermoresisitivity measurements at temperatures between 450 and 500° C.

In the case of the quaternary alloy with a composition approaching that of our alloy, the first stage of precipitation was indirectly demonstrated by Peters and Cupp [35]. This was done by measuring the resistivity of 20° C after ageing of the specimens at temperatures below 450° C. Manenc *et al.* [36] have shown the existence of coherent domains, whose presence is proved by satellite lines close to the diffraction lines of the martensite in the alloy Fe–7.4 Ni–7 Mn–3.5 Ti (at. %). The same phenomenon was observed but was much less distinct in the case of the alloy 70.42 Fe–17.74 Ni–8.83 Co–3.01 Mo (at. %). Again Thomas *et al.* [37] have shown the existence of coherent zones of hexagonal structure, above 20 Å in diameter by transmission electron microscopy on thin foils.

We therefore carried out a systematic study of the preprecipitation by small-angle X-ray scattering (SAS) which should be able to provide more precise information about the size and shape of the zones and the interference between them [38]. Moreover, it seemed interesting to compare the behaviour of the high purity quaternary alloy Fe–Ni–Co–Mo with the industrial maraging steel [39].

Firstly, Mössbauer spectroscopy has shown that the original martensite before any ageing treatment whatsoever, presents clusters of Mo [40]. Considering the clusters to be spherical, we found, using small angle scattering of X-rays that they have a radius of about 5 to 6 Å.

TABLE III

T(°C)	Step	n	$k(t^{-n})$	$k(t^{-1})$
386	I	0.77	0.18	0.11
408	I	0.71	0.34	0.22
426	I	0.52	0.64	0.42
455	I	0.40	0.79	0.56
455	II	0.60	0.15	0.04
482	I	0.76	1.14	0.55
482	II	0.70	0.15	0.06
506	II	0.93	0.64	0.91
530	II	1.15	1.32	1.20

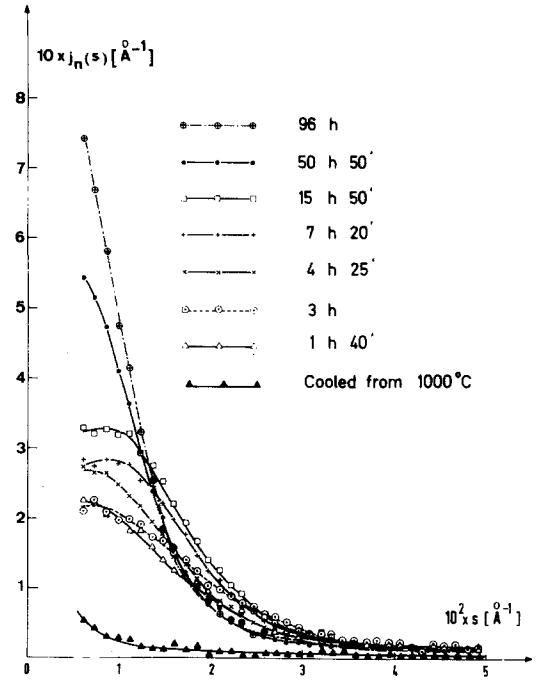

Figure 33 Small-angle scattering curves for the synthetic maraging steel observed for different ageing times at 414° C.

The SAS curves of the alloy, aged for increasing time intervals at 414° C are represented on Fig. 33. We note the existence of a SAS ring. In the exponential approximation of Guinier, we have deduced the evolution of the gyration radius of the zones as a function of time, as shown in Fig. 34. After 15 h coalescence of the zones is produced, corroborated by a decrease of the ratio S/V (specific area of the zones) of the Porod's law

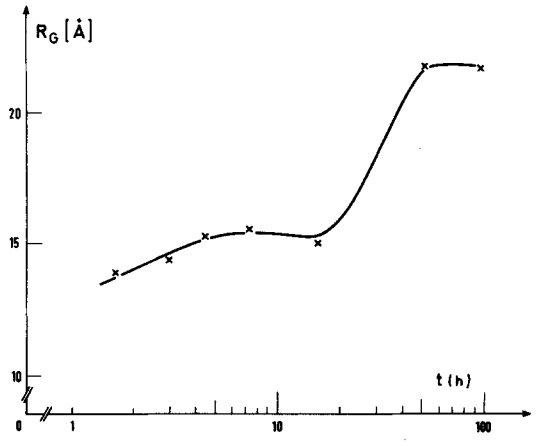

Figure 34 Variation of the gyration radius of the synthetic maraging steel as a function of the ageing time at 414° C.

[41]. This is expressed in linear collimation, by the expression:

$$\lim_{s\to\infty} j_n(s)\cdot s^3 = \frac{1}{16\pi^2}\left(\frac{\rho-\rho_0}{\bar{\rho}}\right)^2 \frac{S}{V}$$

where ρ = electron density of the zone rich in Mo, ρ_0 = electron density of the matrix poor in Mo, $\bar{\rho}$ = average electron density of the alloy (Fig. 35). This coalescence of the zones after 15 h is confirmed by a diminution in the hardness.

In the initial stages of ageing ($t = 3$ h), Porod's law is not obeyed, and this could be associated with the existence of non-globular zones. These results seem to be confirmed by the streaking of diffraction spots on the diffraction pattern (Fig. 36). For longer durations of time ($t > 7$ h), the zones are practically spherical. Moreover, an examination of the SAS curves indicates that the heterogeneisation of the martensite solid solution is not brought about by a process of spinodal decomposition.

In the case of industrial steel, the diffusion curves also show a modulation, reflecting the interference between the wavelength diffused by the coherent zones present in the steel for ageing temperatures of the order of 400° C [39].

5. General conclusions

We have shown that the metastable diagram for the Fe–Ni alloy by Jones and Pumphrey could be extrapolated to the ternary systems Fe–Ni–Co and Fe–Ni–Mo. The austenitic transformation of these alloys is brought about in one or several successive steps according to the Co content and/or the Mo content, and according to the rate of heating. At moderate heating rates (300° C h^{-1}), this transformation is brought about by a preponderantly diffusional mechanism. The difference in the proportion of Ni and/or Mo in the two phases formed, i.e. martensite poor in Ni or (Ni + Mo) and austenite enriched in these elements, is much greater at the beginning of the transformation M → γ.

For alloys containing Mo, the transformation M → γ is conditioned by the phenomena of pre-precipitation and precipitation taking place before the point A_{s_0}. In fact, for the synthetic Fe–Ni–Co–Mo alloy, and the industrial steel, the small-angle scattering of X-ray curves show a modulation. This suggests the existence of Mo zones, distributed regularly in the martensite matrix poor in Mo, in the hypotheses of a model of zones of two electron

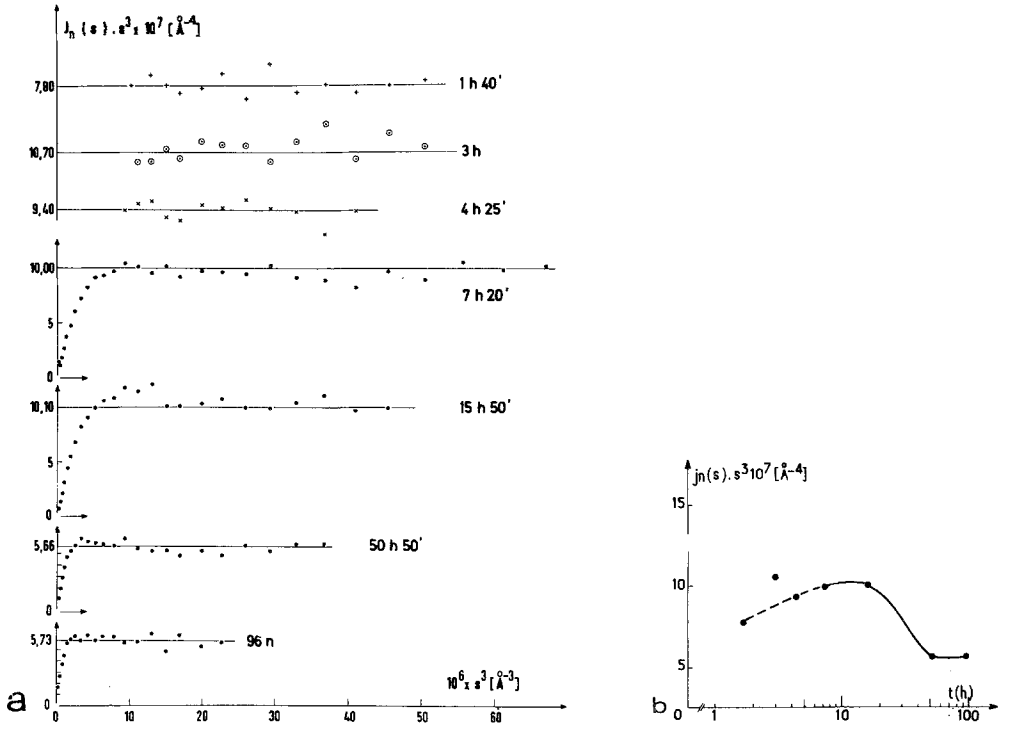

Figure 35 (a) Variation of the function $j_n(s)\ s^3$ as a function of s^3 for the synthetic maraging steel showing that the Porod's law is well obeyed after 7 h of ageing. (b) Variation of the function $j_n(s)\ s^3$ versus time for the synthetic maraging steel.

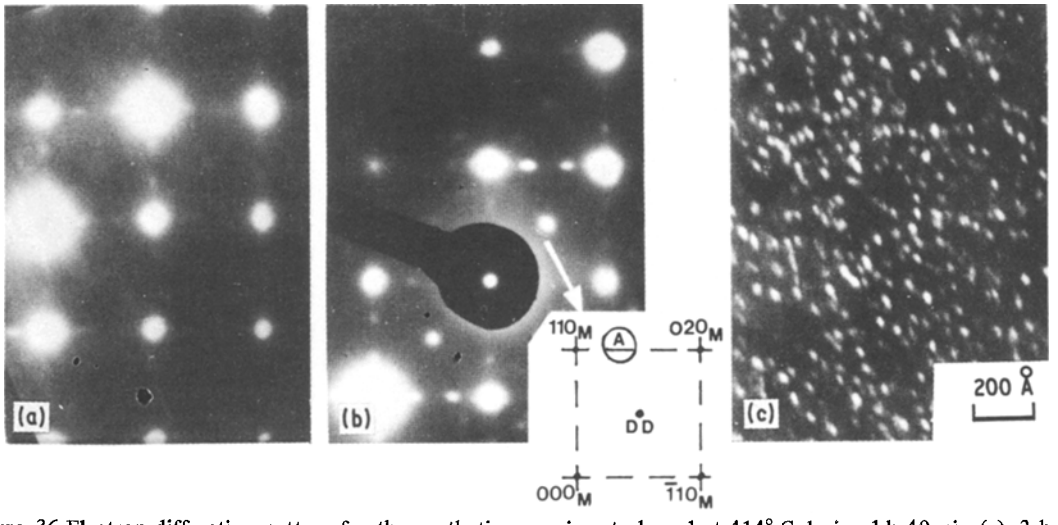

Figure 36 Electron diffraction pattern for the synthetic maraging steel aged at 414° C during 1 h 40 min (a); 3 hours (b); dark field for the spot A of diagram b (c).

densities [38]. For these two steels, the austenitic transformation in two steps explains the evolution of zones rich and poor in Mo respectively.

References

1. R. F. DECKER, J. T. EASH and A. J. GOLDMAN, *A.S.M., Trans.* **55** (1962) 58.
2. A. GOLDBERG and J. WELD, *ibid* **47** (5) (1968) 199.
3. A. GOLDBERG, *ibid* **61** (1) (1968) 199.
4. G. A. BERJNEV, V. G. GROVALD, *Metal. I. Term. Obra. Metal* **6** (1968) 15.
5. L. N. BELYAKOV, V. L. NIKOL'SKAYA, S. S. RYZHAK, *ibid* **6** (1968) 26.
6. G. MAEDER, G. CIZERON, P. LACOMBE, *Mém. Sci. Rev. Met.* **LXVI** 3 (1969) 179.

7. P. LEGENDRE, X. WACHE, *ibid* **LXI** 1 (1964) 33.
8. J. P. THEVENIN, Thèse de 3ème Cycle (1966) Paris.
9. J. PITAUD, *Revue du Nickel* **29** (1963).
10. *Idem, ibid,* **28** 2 (1962).
11. C. SERVANT, Thesis, Doctorat d'Etat, Université Paris-Sud, Orsay (1972).
12. F. W. JONES and W. I. PUMPHREY, *J. Iron Steel Instit.* **163** (1949) 121.
13. L. KAUFMAN and M. COHEN *Journal of Metals* (1956) 1393.
14. W. S. OWEN and E. A. WILSON, Physical properties of martensite and bainite", Edited by PERCY LUND, (Humphries and Co, London and Bradford, 1965).
15. R. G. B. YEO, *Trans. A.S.M.* (1964) 57.
16. C. M. WAYMAN, "Physical properties of martensite and bainite" edited by Perey Lund, (Humphries and Co, London and Bradford, 1965).
17. S. JANA and C. M. WAYMAN, *Trans. AIME* **239** (1967) 1187.
18. J. F. BREEDIS and C. M. WAYMAN, *ibid* **224** (1962) 1128.
19. K. W. ANDREWS, D. J. DYSON, S. R. KEOWN, "Electron diffraction patterns", London, (Adam Hilger Ltd., London, 1968).
20. J. M. MARDER and A. R. MARDER, *Trans. A.S.M.* **62** (1969).
21. G. R. SPEICH, *Trans. AIME* **245** (1969) 2553-65.
22. F. RHINES, "Phase-diagrams in metallurgy", (McGraw-Hill, New York, 1956).
23. C. SERVANT et G. CIZERON, *Mèm. Sci. Rev. Metal.* **LXVI** 7-8 (1969).
24. M. HANSEN, "Constitution of binary alloys", (McGraw-Hill, New York, 1958).
25. A. J. BAKER, P. R. SWANN, *Trans. A.S.M.* **57** (1964) 1008.
26. G. MAEDER, Thesis, Doctorat d'Etat, Université Paris-Sud, (1975).
27. M. HANSEN, "Constitution of binary alloys", (McGraw-Hill, New York 1958).
28. G. KRAUSS and M. COHEN, *Trans. AIME* **227** (1963) 278.
29. L. PRIESTER, Thesis, Doctorat d'Etat, Université Paris-Sud (1972).
30. C. SERVANT, G. MAEDER, G. CIZERON et P. LACOMBE, *Mèm. Sci. Rev. Met.* **LXIX** 4 (1972) 234.
31. J. E. BURKE, "The Kinetics of Phase Transformations in Metals", (Pergamon Press, Oxford, 1965).
32. A. H. COTTRELL and B. A. BILBY, *Proc. Phys. Soc.* **A62** (1949) 49.
33. S. HARPER, *Phys. Rev.* **83** (1951) 209.
34. C. SERVANT, G. MAEDER, G. CIZERON et P. LACOMBE, *Mèm. Sci. Rev. Met.* **4** (1971) 201.
35. D. T. PETERS and C. R. CUPP, *Trans. AIME* **236** (1966) 1420.
36. J. MANENC et J. BOURGEOT, *Acta Met.* **17** (1969) 891.
37. J. BOURGEOT, P. MAITREPIERRE, J. MANENC and B. THOMAS, Fifth International Materials Symposium, University of California, Berkeley, California, 1971.
38. A. GUINIER et G. FOURNET, "Small-Angle Scattering of X-rays", (John Wiley, New York, 1955).
39. C. SERVANT, G. MAEDER and G. CIZERON, *Met. Trans.* **6A** (1975) 981.
40. J. BOURGEOT, P. MAITREPIERRE, J. MANENC and B. THOMAS, Communication presented in Full Meeting of "Société Française de Métallurgie" (1972).
41. G. POROD, *Kolloid. Z.* **124** (1951) 83; **125** (1952) 51; **133** (1953) 16.
42. NAM BUI et F. DABOSI, *Le cobalt* **57** (1972) 192.

Received 20 December 1976 and accepted 10 January 1977.